crystals

MDPI

Article

Effect of Curing Conditions on the Strength Development of Alkali-Activated Mortar

Lijuan Kong [1,2,3,*], Zirui Fan [2], Wenchen Ma [2], Jiatao Lu [2] and Yazhou Liu [2]

[1] State Key Laboratory of Mechanical Behavior and System Safety of Traffic Engineering Structures, Shijiazhuang Tiedao University, Shijiazhuang 050043, China
[2] School of Materials Science and Engineering, Shijiazhuang Tiedao University, Shijiazhuang 050043, China; fanzirui@stdu.edu.cn (Z.F.); 20182851@student.stdu.edu.cn (W.M.); 20182848@student.stdu.edu.cn (J.L.); liuyazhou@stdu.edu.cn (Y.L.)
[3] Hebei Key Laboratory of Advanced Materials for Transportation Engineering and Environment, Shijiazhuang Tiedao University, Shijiazhuang 050043, China
* Correspondence: klj@stdu.edu.cn

Abstract: In this study, the strength development and microstructure evolution of alkali-activated fly ash (AAF), granulated blast furnace slag (AAG), and metakaolin (AAM) mortars under standard curing, steam curing, and oven curing conditions were investigated. The results show that 80 °C steam curing was more suitable for AAF mortar. Although oven curing was not as good as steam curing under the same temperature, the water evaporation increased the volume density of the N-A-S-H gel and refined the pore structure. For AAG mortar, the strength developed according to a Boltzmann function with time under steam curing conditions, which increased rapidly in the first 8 h, but grew little after about 15 h. Moreover, the strength development was severely limited by steam curing at 60 °C, and decreased under oven curing conditions due to the formation of microcracks that were induced by temperature stress and chemical shrinkage. For AAM mortar, the strength developed according to an Allometric power function with time under steam curing conditions, and the N-A-S-H gel formed in AAM had a higher polymerization degree and denser structure compared to that in AAF. The compressive strength of AAM mortar was 31.7 MPa after 80 °C steam curing for 4 h, and the standard curing time required to reach the same strength was less than 24 h, indicating that the standard curing was more suitable.

Keywords: alkali-activated mortar; strength; standard curing; steam curing; oven curing

Citation: Kong, L.; Fan, Z.; Ma, W.; Lu, J.; Liu, Y. Effect of Curing Conditions on the Strength Development of Alkali-Activated Mortar. *Crystals* **2021**, *11*, 1455. https://doi.org/10.3390/cryst11121455

Academic Editors: Chongchong Qi, Payam Hosseini and Baoguo Han

Received: 4 November 2021
Accepted: 21 November 2021
Published: 25 November 2021

1. Introduction

Alkali-activated material is a new type of cementitious material that has gained much attention in recent years [1,2]. It is made of silica-rich aluminum minerals (i.e., metakaolin, fly ash, slag, etc.) and alkali solution [3–5]. This material is environmentally friendly, and has more excellent mechanical and durability properties than traditional cement [6,7], and thereby has promising application prospects [8]. Moreover, the reactions including "dissolution, monomer reconstruction and polycondensation" [9] can occur at room temperature or high temperature (usually below 100 °C), and then a compact and stable three-dimensional network structure is formed [10].

As alkali-activated material is completely different from traditional cement in terms of raw materials, preparation technology, and reaction mechanism, some known mechanisms such as the influence of curing methods on the strength of concrete are not fully applicable. For cement concrete, the compressive strength from standard curing for 7 d can reach 70% of 28 d strength. Although steam curing for 16–18 h can also reach 70–80% of 28 d strength [11], it is adverse for long-term strength development and durability. Therefore, Aldea [12] proposed that the standard curing is the best for concrete durability, but steam curing is preferable to pressure steaming if the concrete strength needs to be developed rapidly.

For alkali-activated concrete (AAC), increasing curing temperature can also promote the alkali-activated reaction, improve the porous structure, and reduce microcracks [13], thereby increase the strength [14,15]. Some studies have found that the strength of alkali-activated fly ash (AAF) concrete at 80 °C steam curing is higher than that in 50 and 65 °C environments [16]. However, when the curing temperature exceeds 120 °C, the growth rate of AAF concrete strength is extremely low. Moreover, the steam curing time should be controlled within 16 h, because if that time is exceeded, the strength growth rate is not significant [17]. Jamdade [18] found that the strength of AAF concrete is the highest when curing at 90 °C for 18–24 h. Some studies reported that the optimal curing temperature of AAC is 80 °C [19]. Zhang et al. [20] compared the strength development law of AAF concrete under standard curing, 80 °C steam curing, and 150 °C autoclaved curing, and found that the latter has the greatest influence on the strength of concrete. The compressive strength of AAF concrete can reach 47.5 MPa after only 2 h autoclaved curing; however, the energy consumption is the highest and the operation is inconvenient. In an oven curing environment, the strength of AAF concrete also increased with the increase in temperature, but dropped suddenly at 150 °C and some cracks appeared [21]. During the steam curing process, it was also found that the resistance to chloride ion penetration of AAC decreased with the increase in curing temperature [22], indicating the degradation of the microstructure. For alkali-activated granulated blast furnace slag (AAG) concrete, the early strength increased obviously with the increase in curing temperature, but returned to the standard curing level after 28 d [23].

Curing is the important link to ensure the quality and performance of concrete, especially for AAC. At present, most studies focus on the influence of curing temperature and methods on the strength of AAF concrete. There is almost no research on the effect of curing on the strength development and reaction mechanism of the other AAC. Therefore, fly ash (FA), granulated blast furnace slag (GBFS), and metakaolin (MK) were used to prepare AAC in this work, and the strength development and the relationship between them under standard curing, steam curing, and oven curing were studied, in addition to the evolution of their microstructure. The results obtained are expected to provide some theoretical guidance for the curing production of AAC.

2. Experiment

2.1. Raw Materials and Specimen Preparation

2.1.1. Raw Materials

Grade II FA from Huaneng Shangan Power Plant, S95 GBFS from Shijiazhuang Lingshou Zhongshan Cement Group, and MK from Gongyi Chenyi wear resistant material company were used in this study to prepare alkali-activated mortar. Their chemical compositions were determined by X-ray fluorescence spectrometer (XRF) as shown in Table 1. The alkali activator was composed of sodium silicate (Na_2SiO_3) solution with a modulus of 3.25 and 98 wt% sodium hydroxide (NaOH) particles in proportion, and an alkali content of 13%, which was prepared 1 d in advance. Zhengding river sand was used as the fine aggregate with a fineness modulus of 2.65, apparent density of 2690 kg/m^3, and mud content of 1.0%.

Table 1. Chemical composition of raw materials.

Composition wt%	SiO_2	Al_2O_3	CaO	Fe_2O_3	MgO	Na_2O	K_2O	SO_3
FA	49.3	28.5	1.86	3.96	0.94	0.69	2.6	0.51
GBFS	29.8	13	38.7	0.3	7.71	0.35	0.39	2.3
MK	54.5	43.1	-	0.48	0.07	0.67	0.2	0.35

2.1.2. Specimen Preparation

The water–binder ratio and paste–aggregate ratio of the three groups were 0.35 and 0.68 respectively. Firstly, 537 g FA/GGBFS/MK and 1350 g sand were put into a cement mortar mixer and stirred at low speed for 5 min, and then 306.7 g alkali activator and 67.7 g

water were added slowly and stirred for 10 min. The mixed alkali-activated mortar was put into 40 mm × 40 mm × 160 mm test mold and vibrated for 1 min. Finally, the surface was covered with plastic wrap and placed in different environments for curing until the test age. In addition, the paste specimens with the same water–binder ratio and the same curing condition were prepared for the microscopic test.

2.2. Curing Condition

Five different curing conditions were set to study the strength development of the mortars, and the alkali-activated FA/GGBFS/MK mortars under different curing environments were designated as F/G/M + B/Z60/Z80/H60/H80.

- ➢ Standard curing (B): The specimens were placed in a 20 ± 5 °C environment for 24 h after casting, then they were demolded, numbered, and placed into a standard curing room (temperature = 20 ± 2 °C, relative humidity ≥ 95%) until a specified age;
- ➢ Steam curing (Z): After casting, the specimens were directly steam cured at 60 °C (Z60) and 80 °C (Z80) until a specified age;
- ➢ Oven curing (H): The specimens were first placed in an 80 °C steam curing box for 6 h to reach a certain strength and then demolded, numbered, and moved to the oven at 60 °C (H60) and 80 °C (H80) for curing until the test age.

2.3. Test Method

2.3.1. Strength Test

The compressive strength of alkali-activated mortars was tested according to the Chinese standard of "Cement mortar Strength Test Method (ISO method)" (GB/T 17671), and the test ages of standard curing and steam/oven curing were 1, 3, 7, 14, and 28 d and 2, 4, 6, 8, 24, and 48 h, respectively.

2.3.2. Fourier Transform Infrared Spectroscopy (FTIR)

A Nicolet Vatar-330 Fourier infrared spectrometer was used to test and analyze the products of alkali-activated samples after different curing conditions. The spectra were gathered for wavenumbers between 400 and 4000 cm^{-1}. After grinding and drying, the sample powder was mixed with potassium bromide based on a ratio for tablet pressing and testing.

2.3.3. Scanning Electron Microscopy-Electron Dispersive Spectrometry (SEM-EDS)

The micro-morphology and elemental distribution of clean slurry samples under different curing conditions were characterized by S-4700 SEM-EDS (Hitachi). The sample size was about 1 cm^3, and it was dried and gold coated before testing.

2.3.4. Brunner Emmet Teller (BET) Measurement

A 3H-2000PS1 specific surface and pore size analyzer made by Beijing Best Company was used to measure the specific surface area, cumulative pore volume, and pore size distribution [24] of alkali-activated samples under different curing conditions. Before testing, samples of about 1 g were collected and pretreated by heating at 90 °C and vacuum-degassing for 9 h.

3. Results and Discussion

3.1. Strength Test

3.1.1. Standard Curing

Figure 1 shows the fitting results of the compressive strength development of alkali-activated mortars under standard curing. It can be seen that all the fitting lines were positively correlated in a linear relation. The y-intercept of the fitting line of FB was negative, indicating that its initial compressive strength is extremely low, and it began to produce strength after 40 h standard curing based on the function calculation, and the compressive strength at 3 d is only 1.3 MPa due to the low activity of fly ash [25]. For GB

and MB specimens, their initial strengths were high, and after standard curing for 1 d, the compressive strengths were 48.0 and 50.6 MPa, reaching 57% and 64% of their 28 d strength, respectively. However, the compressive strength of ordinary cement mortar after 3 d standard curing only reaches 50% of its 28 d strength [11]. This indicates that the strength of GB and MB developed faster in early age; moreover, their strength continued to increase with the increase in curing time. The slopes of the three fitting lines had slight differences, among which GB had the highest slope, followed by FB and MB. The compressive strength of the GB specimen after 28 d standard curing was 83.6 MPa, indicating that standard curing was more beneficial to the strength development of AAG mortar. However, the AAF mortar was not suitable for standard curing. The strength of GB and MB specimens was about 2.5 times that of FB after standard curing for 28 d.

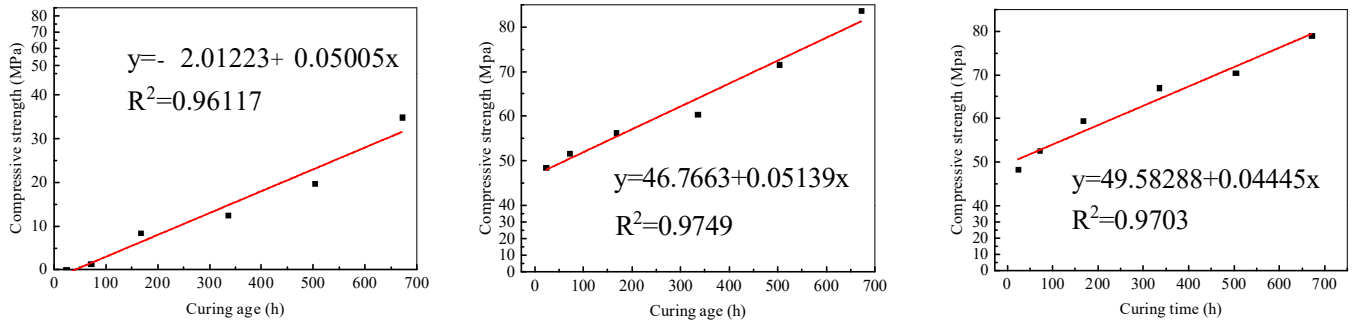

Figure 1. Fitting results of compressive strength of alkali-activated mortars under standard curing: (**a**) FB; (**b**) GB; (**c**) MB.

3.1.2. Steam Curing

Figures 2 and 3 show the fitting results of the compressive strength of alkali-activated mortars under steam curing at 60 and 80 °C. For AAF mortars, the compressive strength of FZ60 also increased linearly with time in 60 °C steam environment, but both the y-intercept and slope of the fitting line are larger than that under the standard curing condition, indicating that steam curing is more favorable to the growth of the initial and later strength of AAF mortar by comparison with standard curing, as shown in Figure 2a. When the temperature increased from 60 to 80 °C, steam curing more significantly promoted the strength development of AAF specimens, as shown in Figure 3a. The compressive strength of FZ80 developed according to an Allometric function with time, and reached 1.8 MPa after only 2 h steam curing, exceeding that of standard curing for 3 d, and close to that of 60 °C steam curing for 8 h. Therefore, AAF mortar was more suitable for 80 °C steam curing.

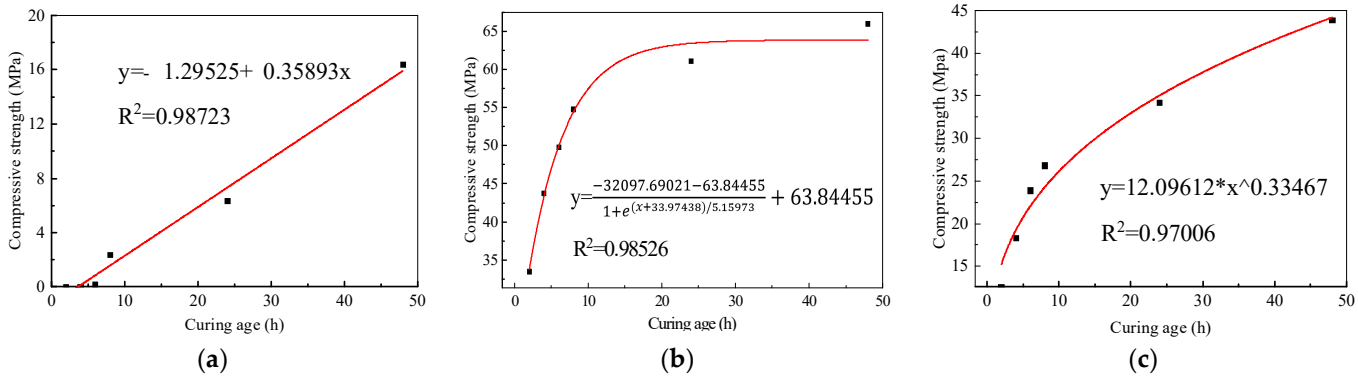

Figure 2. Fitting results of the strength of alkali-activated mortars under steam curing at 60 °C: (**a**) FZ60; (**b**) GZ60; (**c**) MZ60.

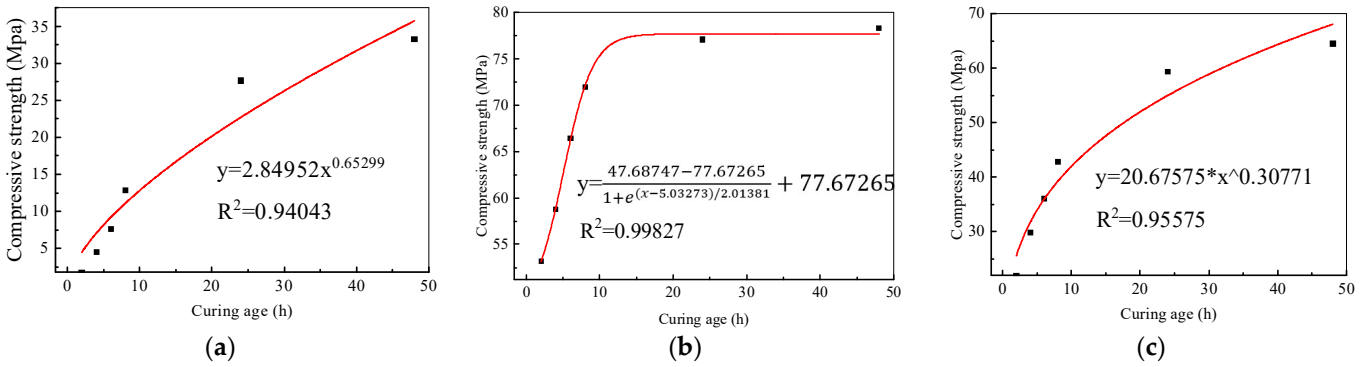

Figure 3. Fitting results of the strength of alkali-activated mortars under steam curing at 80 °C: (**a**) FZ80; (**b**) GZ80; (**c**) MZ80.

For AAG mortars, both the compressive strengths developed according to a Boltzmann function with time under 60 and 80 °C steam curing conditions, as shown in Figures 2b and 3b. The strength of GZ60 increased rapidly in the first 8 h and reached the maximum value after 20 h. Furthermore, both the initial and maximum strengths increased with the rise in curing temperature, and the curing time to reach the maximum strength of GZ80 was only 12 h. However, the maximum strengths of GZ60 and GZ80 under steam curing conditions were 22% and 7% lower than that of GB under standard curing conditions for 28 d, respectively. Obviously, although the steam curing can accelerate the strength growth of AAG mortar, it will hinder the development of strength to a higher value. From the perspective of reaction kinetics, the increase in temperature reduces the activation energy of the reaction and speeds up the alkali-activated reaction rate [26], but the chemical equilibrium moves in the opposite (endothermic reaction) direction, which leads to the reduction in gel products and structural density. In addition, the gel rapidly formed on the surface of the slag particles without diffusion, resulting in uneven product distribution [27]. All of the above factors would cause the slow strength development of AAG mortar in the long term.

For AAM mortar, the compressive strength developed according to an Allometric function with time under both 60 and 80 °C steam curing conditions, as shown in Figures 2c and 3c. Their strength increased rapidly, not only in the first 8 h, but also in the later period. The effect of curing temperature on the strength of AAM mortar was similar to that of the other alkali-activated mortars.

By comparing the sensitivity of the three alkali-activated mortars to steam curing, it was found that the strength of AAG mortar developed the fastest in the first 8 h but increased little thereafter, whereas the strength of AAF and AAM mortars still underwent a substantial rise in 8–48 h. Therefore, it is suggested that 80 °C steam curing should be adopted to increase the early strength of alkali-activated mortars. Regarding AAG mortar, the steam curing time should be controlled within 12 h to reduce energy consumption; for AAF and AAM mortar, the steam curing time can be appropriately extended to promote the development of strength.

3.1.3. Oven Curing

Oven curing is also called dry curing, and the essential difference from steam curing is that the relative humidity in the oven is very low. The fresh mortars were first cured under the steam condition for 6 h to form certain strength, and then moved to the oven for further curing. From Figure 4 it can be seen that, in the first 6 h, the compressive strengths of the alkali-activated mortars under both steam and oven curing at 80 °C were the same. When oven curing began, the strength of AAF mortar continued to increase, but its increasing rate was significantly lower than that of the steam curing group. However, instead of increasing, the strengths of AAG and AAM mortar decreased gradually with time. After 48 h curing, the compressive strength of FH80 increased by 127%, whereas those of GH80 and MH80 decreased by 26% and 39%, respectively, compared with the initial oven curing

strength. It is thus clear that the oven curing for a certain time had no adverse effect on the strength development of AAF mortar, but would decrease the strength of AAG and AAM mortars. This is due to the dual effect of oven curing: the high temperature will accelerate the alkali-activated reaction and promote the strength growth; conversely, the generation of microcracks by drying shrinkage will reduce the strength. For AAF mortar, the positive effect is more significant due to the low activity of FA, whereas for AAG and AAM mortars, the negative effect is dominant. Moreover, as the compressive strength of AAG mortar reached 66.4 MPa after 6 h steam curing, its dense structure had certain resistance to the internal stress and volume shrinkage, so the decline rate of the strength was lower than that of AAM mortar. Figure 4 also indicates that the strength of AAG mortar developed rapidly in the first 8 h under the steam curing condition, whereas that of AAF and AAM mortars had a larger increase after steam curing for 8 h.

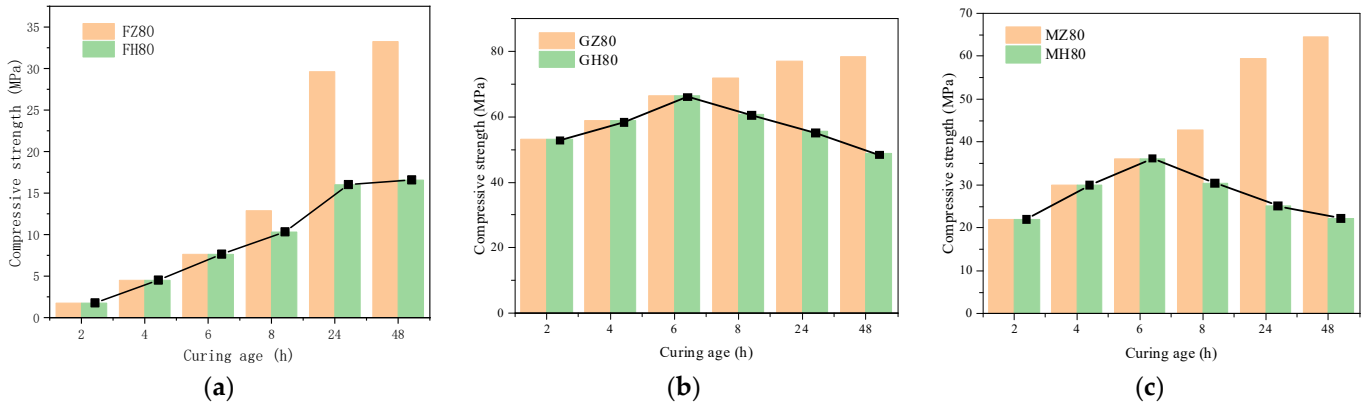

Figure 4. Strength of alkali-activated mortar under oven and steam curing conditions: (**a**) FH; (**b**) GH; (**c**) MH.

3.1.4. Strength Correlation between Standard Curing and Steam Curing

Although steam curing can shorten the curing period and speed up the construction progress, it requires higher energy consumption and generates environmental pollution, in addition to adversely affecting the properties of concrete. Therefore, it is necessary to choose a suitable curing method and control the reasonable curing time according to the characteristics of raw materials. In this study, the strength development laws of three alkali-activated mortars under standard curing and steam curing conditions were compared, as shown in Figure 5, in order to find the corresponding relationship between them and guide their production. Furthermore, based on the strength of alkali-activated mortars after 80 °C steam curing for 4 and 24 h, the curing time required to reach the same strength for each curing system was calculated. The results are listed in Table 2.

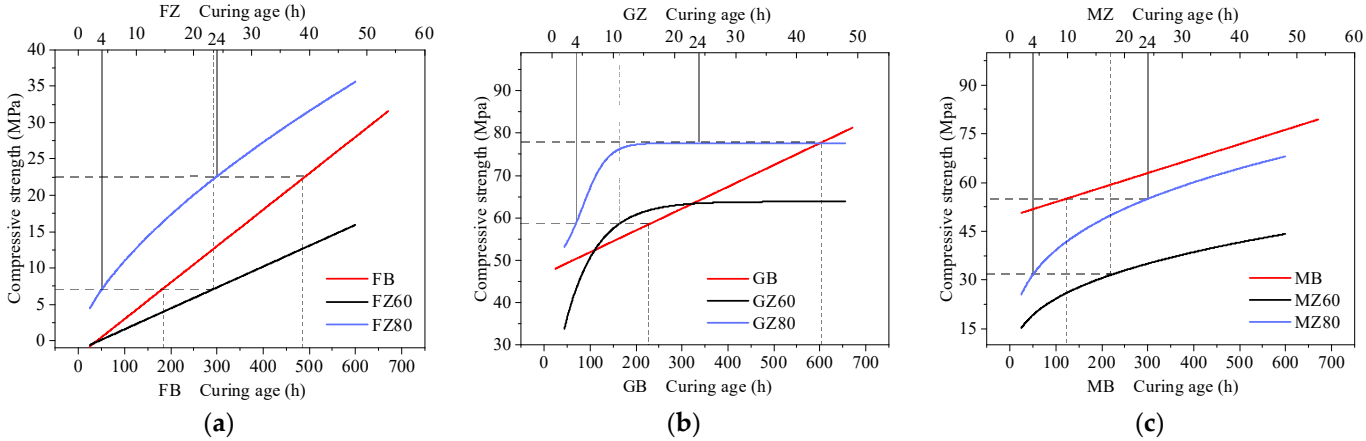

Figure 5. Correlation between strength of alkali-activated mortar under standard curing and steam curing: (**a**) AAF; (**b**) AAG; (**c**) AAM.

Table 2. Relationship between the strength and curing time of alkali-activated mortar.

No.	Steam Curing at 80 °C (h)	Strength (MPa)	Standard Curing (h)	Steam Curing at 60 °C (h)
AAF	4	7.0	181	23
	24	22.7	494	67
AAG	4	58.9	236	11
	24	77.7	603	-
AAM	4	31.7	<24	18
	24	55.0	121	92

Comparative analysis showed that the strength of AAF mortars after 4 h steam curing at 80 °C reached 7.0 MPa, which was equivalent to that after 23 h steam curing at 60 °C and 181 h standard curing; and the strength of AAF mortar after 24 h steam curing at 80 °C reached 22.7 MPa, which was equivalent to that after 67 h steam curing at 60 °C and 494 h (20.6 d) standard curing. Obviously, the AAF mortar was more suitable for steam curing. For AAG mortar, the steam curing at 60 °C would severely limit the strength development, and its maximum strength was only equivalent to the strength under standard curing for about 14 d, whereas the strength after 12 h steam curing at 80 °C approached that after standard curing for 28 d. For AAM mortar, the strength after 80 °C steam curing for 4 h was 31.7 MPa, whereas the standard curing time required to reach it was less than 24 h, which was greatly reduced compared to the other two alkali-activated mortars, indicating that AAM mortar was more suitable for standard curing.

3.2. Microscopic Test

3.2.1. FTIR Test

To further analyze the influence of curing conditions on AAC, the compositions of alkali-activated paste were tested by FTIR and the results are shown in Figure 6. The absorption bands between 1458.26–1429.71 cm^{-1} and 1024.83–1004.00 cm^{-1} are carbonate (C-O antisymmetric stretching vibration [28]) and Si-O-T (T=Si/Al) asymmetric stretching vibration, respectively. The absorption peaks at 955 and 1640 cm^{-1} are Si-O-M (M=Ca/Al) vibration and H-O-H bending vibration, respectively [29].

From the results shown in Figure 6a, it can be seen that the positions and shapes of the characteristic peaks of AAF after 7 d standard curing and 8 h steam curing were similar, but the Si-O-T absorption peak of the latter slightly shifted to the left, indicating that the N-A-S-H gel of AAF formed in a short time under steam curing condition was more stable. When the AAF was cured in an oven, the depth of the Si-O-T absorption peak increased compared to that in the steam curing at the same temperature, which indicates the larger volume density of the N-A-S-H gels generated. It is inferred that the water evaporation during the polycondensation process caused by oven curing would promote the alkali-activated reaction, and the shrinkage of the gel pores also led to the increase in the polymerization degree. Both of these factors resulted in the increase in the intensity of Si-O-T absorption peak. In addition, all the samples had a small carbonate absorption peak, which may be because carbonization occurred between the CaO in fly ash and surplus OH^- in alkali solution. The difference was that the C-O absorption peak of oven curing samples moved 22.74 cm^{-1} to the left compared with other samples, indicating that the $CaCO_3$ generated under the oven curing condition was more stable. However, most of the OH^- participated in the alkali-activated reaction, and only a small amount was left to be carbonated, so the intensity of the C-O absorption peak of oven curing samples was lower. Comparing of Figure 6a,b shows that with the increase in curing time, the position of the Si-O-T absorption peak of AAF moved to the high wavenumber region, and the shape became deeper and sharper. This indicates that the N-A-S-H gel generated with a long chain structure became more stable and ordered, whereas its absorption peaks at 1640 cm^{-1} after 24 h oven curing became very flat, indicating that little water was retained, due to evaporation.

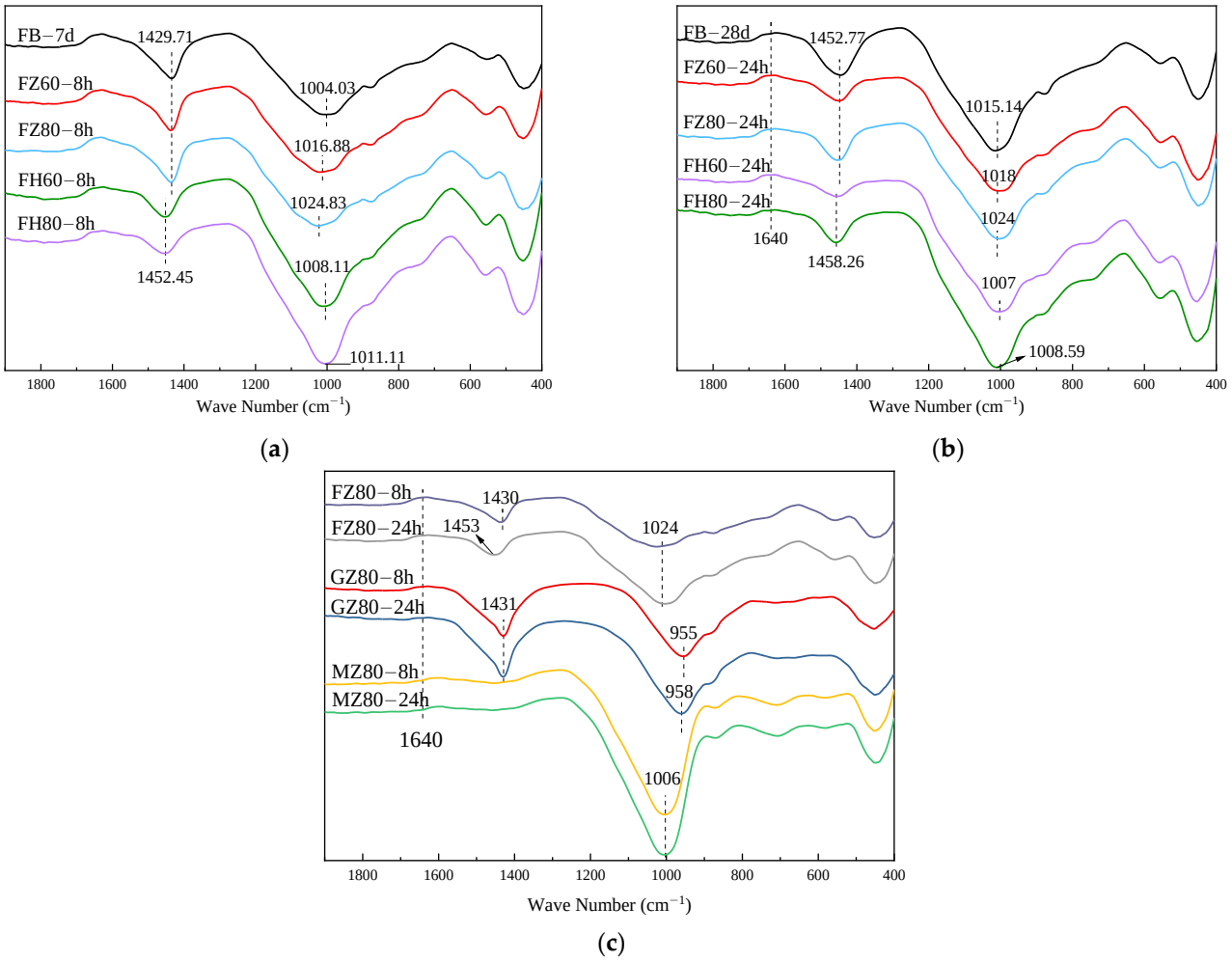

Figure 6. FTIR test results: (**a**) AAF after 7 d/8 h curing; (**b**) AAF after 28 d/24 h curing; (**c**) AAC after 80 °C steam curing.

Figure 6c shows the test results of three alkali-activated specimens under the 80 °C steam curing condition. The intensity of the carbonate absorption peak of GZ80 clearly increased and the peak shape became sharper, which is due to the high CaO content in GBFS. In contrast, there was almost no carbonate absorption peak for MZ80, which belonged to the calcium free cementitious system. Moreover, the intensities of the Si-O-M absorption peak of GZ80-8 h and the Si-O-T absorption peak of MZ80-8 h were higher than that of FZ80-8 h, indicating that the AAF specimen had a poor gel structure. It should be noted that the absorption peak positions of GZ80 and MZ80 samples were almost unchanged when the curing time increased from 8 to 24 h, and only the depth of the absorption peaks increased significantly. This suggests that the product structure of AAG and AAM had been basically formed after 8 h steam curing. With the increase in curing time, only the volume density of C-(A)-S-H gel and N-A-S-H gel changed, and not the long chain structure of the products.

3.2.2. SEM-EDS Test

Figure 7 shows the SEM images of the three alkali-activated specimens under different curing conditions. Furthermore, the elements of the representative products were also analyzed and the results are listed in Table 3.

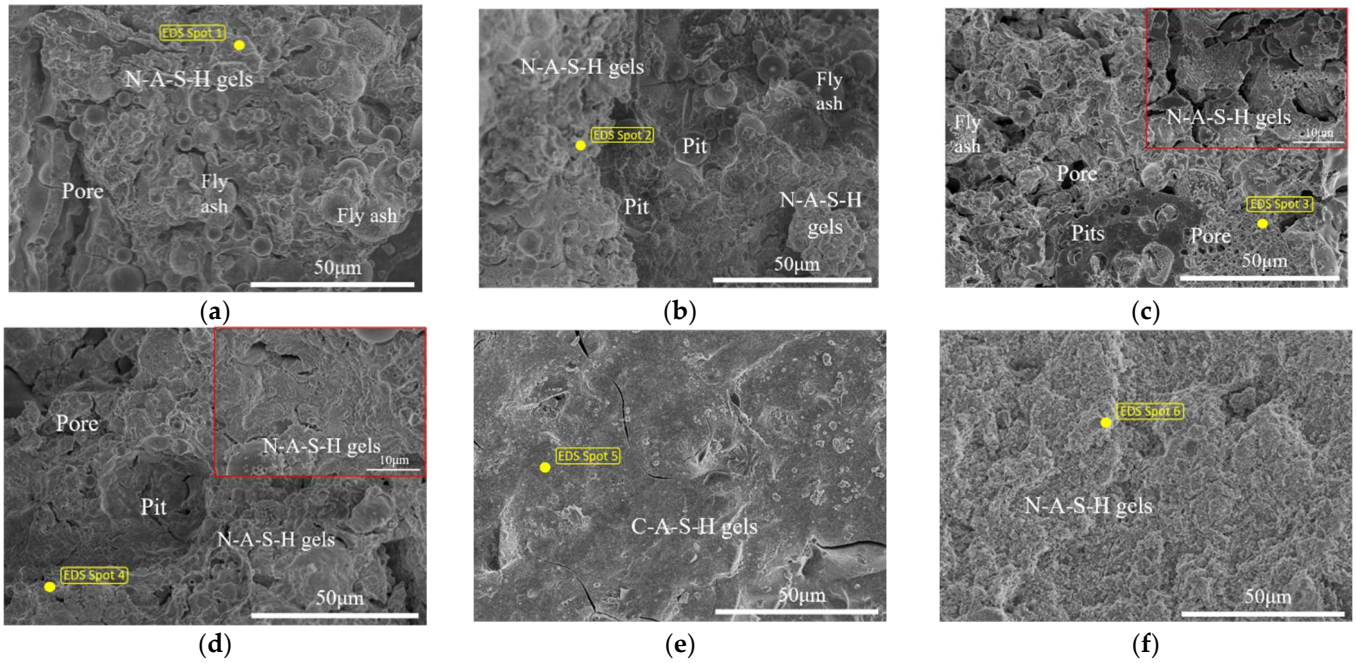

Figure 7. Microstructure of alkali-activated cement under different curing conditions: (**a**) FB-7 d; (**b**) FB-28 d; (**c**) FH80-24 h; (**d**) FZ80-24 h; (**e**) GZ80-24 h; (**f**) MZ80-24 h.

Table 3. Elemental distributions of different alkali-activated specimens.

Element Percentage/%	Spot 1	Spot 2	Spot 3	Spot 4	Spot 5	Spot 6
O	43.76	48.84	46.78	42.84	29.57	39.46
Na	4.16	9.48	8.9	12.87	9.15	7.63
Al	18.16	16.55	16.18	16.08	5.68	22.31
Si	21.25	22.25	24.6	23.26	12.99	24.9
Ca	0.67	2.15	0.79	2.65	23.14	-

As shown in Figure 7a, there were still many spherical fly ash particles on the surface of FB after 7 d standard curing, but the vitreous structure on its surface was dissolved in the high-alkali environment, and chemical forces were formed between the particles by the adhesion of gel products, which were mainly N-A-S-H gels based on the EDS analysis. With the increase in curing time, many pits remained due to the reaction of fly ash particles, and the gels generated were tightly packed, leading to a denser matrix, as shown in Figure 7b. Table 3 shows that all elements of O, Na, and Si at point 2 have higher content compared with that at point 1, indicating that the sodium for charge neutralization and Si-Al bond in N-A-S-H gel increased. Thus, the structure of FB-28 d was more stable, which is consistent with the left shift phenomenon of the Si-O-T absorption peak in FTIR. Furthermore, the Ca content at point 2 also increased, which may be related to the carbonization of Ca^{2+} and OH^- on the gel surface. By comparing Figure 7b,d, it can be seen that the microstructures of FB-28 d and FZ80-24 h were similar, in addition to the distribution of elements at point 2 and 4. This indicates that the gel structure of AAF after 24 h steam curing at 80 °C could be comparable to that after 28 d standard curing. However, a large number of microcracks can be observed on the surface of the specimen after 24 h oven curing at the same temperature (see Figure 7c), which was the direct reason for its lower strength. In addition, the content of Ca at point 3 was lower than that at points 2 and 4, which may be caused by less carbonization on the surface of the gel.

By comparing Figure 7d–f, it can be seen that the structures of GZ80 and MZ80 after 80 °C steam curing for 24 h were significantly denser (almost no holes) than that of FZ80. However, their micro morphology was different. The surface of GZ80-24 h was smooth,

but there were a small number of microcracks due to the large volume shrinkage, whereas that of MZ80-24 h was rough, and the polymerization degree of gel was high. Moreover, the Ca content at point 5 was the highest, reaching 23.14%, indicating the generation of a large amount of C-(A)-S-H gel and $CaCO_3$. For the specimen at point 6, no Ca element was detected but the contents of Si and Al were the highest, indicating that the N-A-S-H gel formed in MZ80 had a higher degree of polymerization compared with FZ80, and was not affected by carbonization. This can be explained as follows: the high vitreous to crystal ratio and calcium content of GBFS led to a strong bond breaking effect, whereas metakaolin has a super volcanic ash effect; thus, both of them had high activity and could rapidly form a dense network structure under the alkali-activated action.

3.2.3. BET Test

A BET test was conducted to analyze the influence of different curing methods on the pore structure of alkali-activated specimens. Nitrogen adsorption-desorption curves and pore size distribution curves of each sample are shown in Figure 8, and the parameters of the pore structure are listed in Table 4. Figure 8b shows that the pore diameters of the samples were mainly distributed in the range of micropores (0–2 nm), among which the most probable aperture (pore diameter that corresponded to the peak value of the distribution curve) of FB-28 d was the smallest (2.0557 nm). However, its nitrogen absorption capacity was the largest, as were the specific surface area and accumulated pore volume, which reached 22.5497 m^2/g and 0.0765 mL/g, respectively; see Table 4. Moreover, the hysteresis loop on the absorption-desorption curve of specimen FB-28 d that was caused by the condensation of nitrogen in the pore channel was the most obvious, as shown in Figure 8a, indicating that its micropores were the best developed. This was followed by specimen MZ80-24 h, the most probable aperture of which was slightly increased to 2.0807 nm. Its nitrogen adsorption capacity was also large, and its specific surface area and accumulated pore volume were 15.9604 m^2/g and 0.0406 mL/g, respectively. This also shows its well-developed micropores and dense structure, which were consistent with the image observed by SEM.

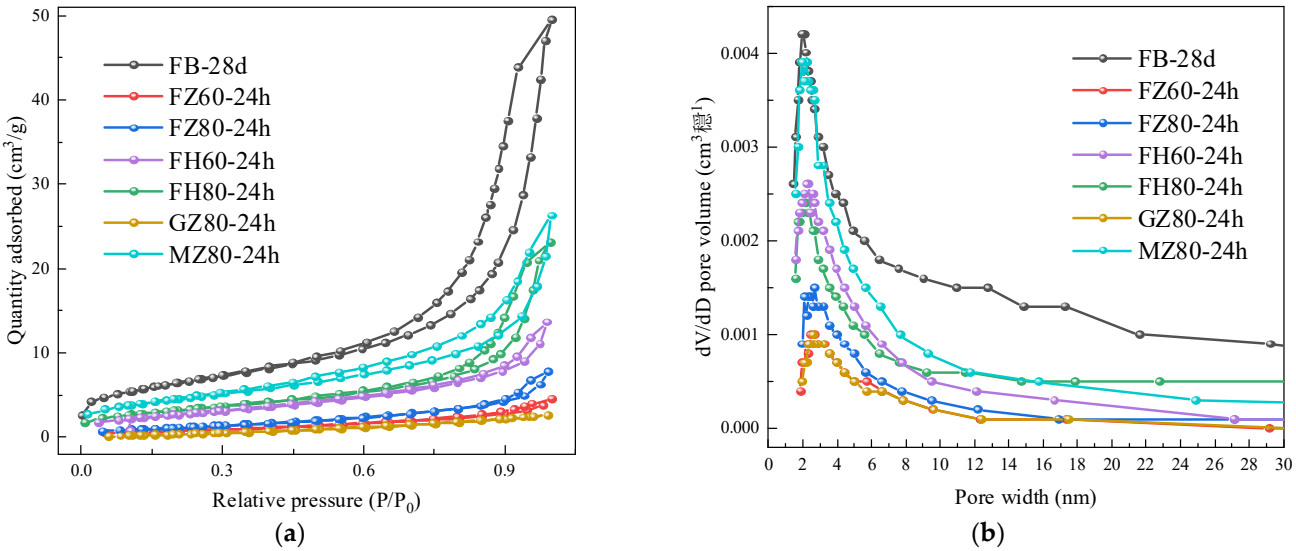

Figure 8. BET test results of alkali-activated cement under different curing conditions: (**a**) AAF after 7 d/8 h curing; (**b**) AAF after 28 d/24 h curing.

Table 4. Pore structure parameters of alkali-activated cement under different curing conditions.

No.	Specific Surface Area (m^2/g)	Cumulative Pore Volume (mL/g)	Most Probable Aperture (nm)
FB-7 d	2.8402	0.0071	3.5467
FB-28 d	22.5497	0.0765	2.0577
FZ60-24 h	2.8129	0.0070	2.5382
FZ80-8 h	1.5801	0.0044	2.9971
FZ80-24 h	4.3889	0.0120	2.4906
FH60-24 h	10.2894	0.0357	2.3356
FH80-8 h	11.7356	0.0316	2.5823
FH80-24 h	13.6304	0.0411	2.2366
GZ80-24 h	3.2026	0.0039	2.5459
MZ80-24 h	15.9604	0.0406	2.0807

In addition, the most probable aperture of specimens FH80-24, FH60-24, FZ80-24, and FZ60-24 was in an increasing order, whereas their nitrogen adsorption capacity, specific surface area, and accumulated pore volume were in decreasing order, confirming once again that oven curing was more advantageous to the formation of the gel structure of AAF than steam curing. Furthermore, with the increase in curing time, the specific surface area and pore volume of AAF increased, and the most probable aperture decreased, indicating that the pore structure of the specimen was refined continuously. For specimen GZ80-24 h, both the specific surface area and accumulated pore volume were the minimum, only 3.2026 m^2/g and 0.0039 mL/g. Little nitrogen entered and was absorbed on the pores, and its adsorption-desorption curve was close to the X-axis. Obviously, the C-(A)-S-H gel generated in specimen GZ80-24 h had more refined pores and a dense structure.

4. Conclusions

(1) Steam curing at 80 °C is more suitable for AAF mortar. Its compressive strength was only 1.3 MPa after 3 d standard curing, whereas it reached 1.8 MPa after 2 h steam curing at 80 °C, close to that under 60 °C steam curing for 8 h. In addition, oven curing for a certain period (48 h) had no adverse effect on the strength development of AAF mortar. Although its strength growth was not as high as that under steam curing at the same temperature, oven curing led to a larger volume density of N-A-S-H gel and better development of gel micropores.

(2) For AAG mortar, the compressive strength increased linearly with time under the standard curing condition, and reached 48.0 MPa after only 1 d standard curing; moreover, it was as high as 83.6 MPa after 28 d. The strength of AAG under the steam curing condition developed according to a Boltzmann function with time, which increased rapidly in the first 8 h, and approached 28 d standard curing strength after 12 h, but grew little after about 15 h. Moreover, the strength development would be severely limited by steam curing at 60 °C. It even decreased under the oven curing condition due to the formation of microcracks due to temperature stress and chemical shrinkage.

(3) The strength of AAM mortar under the steam curing condition developed according to an Allometric power function with time, which not only increased rapidly in the first 8 h, but also had substantial growth in the later period. Furthermore, the N-A-S-H gel formed in AAM had a higher polymerization degree, better micropore development, and denser structure compared to that in AAF. Standard curing is more suitable for AAM, and its compressive strength reached 31.7 MPa after less than 24 h. This, time was remarkably shortened compared with the other two alkali-activated mortars. However, there was a large decrease in the strength under oven curing condition.

Author Contributions: For research articles with several authors, Conceptualization, L.K.; Data curation, Z.F. and W.M.; Investigation, Z.F., J.L. and W.M.; methodology, Y.L. and Z.F.; Writing—original draft preparation, Z.F. and W.M.; writing—review and editing, L.K. and Y.L.; Funding acquisition, L.K.; supervision, L.K. and Y.L.; project administration, L.K. All authors have read and agreed to the published version of the manuscript.

Funding: This study was financially funded by the National Nature Science Foundations of China (51878421), Natural Science Foundation of Hebei Province (E2019210284, E2021210128) and Central Government Foundation for Guiding Local Science and Technology Development (216Z3801G).

Conflicts of Interest: The authors declare no conflict of interest.

References

1. Davidovits, J. Geopolymers and geopolymeric materials. *J. Therm. Anal. Calorim.* **1989**, *35*, 429–441. [CrossRef]
2. Ma, C.-K.; Awang, A.Z.; Omar, W. Structural and material performance of geopolymer concrete: A review. *Constr. Build. Mater.* **2018**, *186*, 90–102. [CrossRef]
3. Ruan, S.; Chen, S.; Zhu, X.; Zeng, Q.; Liu, Y.; Lai, J.; Yan, D. Matrix wettability and mechanical properties of geopolymer cement-polydimethylsiloxane (PDMS) hybrids. *Cem. Concr. Compos.* **2021**, *124*, 104268. [CrossRef]
4. Zhang, M.; Zhao, M.; Zhang, G.; Mann, D.; Lumsden, K.; Tao, M. Durability of red mud-fly ash based geopolymer and leaching behavior of heavy metals in sulfuric acid solutions and deionized water. *Constr. Build. Mater.* **2016**, *124*, 373–382. [CrossRef]
5. Sakulich, A.R.; Anderson, E.; Schauer, C.; Barsoum, M.W. Mechanical and microstructural characterization of an alkali-activated slag/limestone fine aggregate concrete. *Constr. Build. Mater.* **2009**, *23*, 2951–2957. [CrossRef]
6. Ariffin, M.; Bhutta, M.; Hussin, M.; Tahir, M.M.; Aziah, N. Sulfuric acid resistance of blended ash geopolymer concrete. *Constr. Build. Mater.* **2013**, *43*, 80–86. [CrossRef]
7. Gunasekara, C.; Law, D.; Setunge, S. Long term permeation properties of different fly ash geopolymer concretes. *Constr. Build. Mater.* **2016**, *124*, 352–362. [CrossRef]
8. Turner, L.K.; Collins, F.G. Carbon dioxide equivalent (CO_2-e) emissions: A comparison between geopolymer and OPC cement concrete. *Constr. Build. Mater.* **2013**, *43*, 125–130. [CrossRef]
9. Neupane, K. Fly ash and GGBFS based powder-activated geopolymer binders: A viable sustainable alternative of portland cement in concrete industry. *Mech. Mater.* **2016**, *103*, 110–122. [CrossRef]
10. Ng, C.; Alengaram, U.J.; Wong, L.S.; Mo, K.H.; Jumaat, M.Z.; Ramesh, S. A review on microstructural study and compressive strength of geopolymer mortar, paste and concrete. *Constr. Build. Mater.* **2018**, *186*, 550–576. [CrossRef]
11. Li, P. On the relationship between ordinary concrete strength and age under the condition of standard curing. *Water Conserv. Constr. Manag.* **2017**, 53–55. [CrossRef]
12. Aldea, C.-M.; Young, F.; Wang, K.; Shah, S.P. Effects of curing conditions on properties of concrete using slag replacement. *Cem. Concr. Res.* **2000**, *30*, 465–472. [CrossRef]
13. Wang, A.; Zhang, Y.; Zhang, Z.; Liu, K.; Ma, R.; Sun, D. Research progress of geopolymer cementitous material modification for improving durability of concrete. *Mater. Rep.* **2019**, *33*, 2552–2560. [CrossRef]
14. Triwulan, M.; Ekaputri, J.J.; Priyanka, N.F. The Effect of temperature curing on geopolymer concrete. *MATEC Web Conf.* **2017**, *97*, 01005. [CrossRef]
15. Xie, Z.; Li, X. Effect of curing temperature and curing time on compressive strength of fly ash geopolymer concrete. *Concrete* **2014**, 55–58. [CrossRef]
16. Hou, Y.; Wang, D.; Zhou, W. Study of Preparation of Fly Ash-Based Polymer and Its Performance. *Coal Ash China* **2009**, *21*, 3–5. [CrossRef]
17. Naik, S.; Gadhiya, J.; Dhameliya, H. Effect of Duration and Temperature of Curing on Compressive Strength of Fly Ash Based Geopolymer Concrete. *Int. J. Eng. Sci. Res. Technol.* **2016**, *5*, 845–849. [CrossRef]
18. Jamdade, P.K. Effect of temperature and time of curing on strength of fly ash based geopolymer concrete. *Int. J. Inno. Res. Sci. Eng. Technol.* **2016**, *5*, 9269–9274. [CrossRef]
19. Byakodi, A.S.; Srinivas, N. Effect of curing temperature on compressive strength of geopolymer concrete. *Int. J. Rec. Sci. Res.* **2016**, *7*, 12377–12381.
20. Zhang, Y.; Sun, W.; Sha, J.; Lin, W.; Zheng, K.; Liu, S. Preparation, properties and mechanism of fly ash based geopolymer concrete. *J. Build. Mater.* **2003**, *6*, 237–242. [CrossRef]
21. Hake, S.; Damgir, R.; Patankar, S.V. Effect of temperature and curing type on geopolymer concrete. *Int. J. Adv. Res. Sci. Eng.* **2016**, *5*, 1534–1540.
22. Ekaputri, J.J.; Mutiara, I.S.; Nurminarsih, S.; Van Chanh, N.; Maekawa, K.; Setiamarga, D.H.E. The effect of steam curing on chloride penetration in geopolymer concrete. *MATEC Web Conf.* **2017**, *138*, 01019. [CrossRef]
23. Wang, Q.; Zhao, X.; Li, L.; Sui, Z. The influence of early stage curing systems on mechanical properties of slag-based geopolymer concrete. *J. Wuhan Univ. Techno.* **2009**, *31*, 27–30. [CrossRef]
24. Ding, Q.; Jin, H.; Zhang, G.; Yang, J.; Yan, P.; Zhou, P. Effect of C_3A content on microstructure of C_3A-C_3S paste. *B Chin. Ceram. Soc.* **2020**, *39*, 717–723. [CrossRef]

25. Wang, A.; Wang, X.; Sun, D.; Zhu, Y.; Liu, K. Research progress on setting and hardening of geopolymers and their control. *Mater. Rep.* **2021**, 1–17. [CrossRef]
26. Peng, Y.; Guo, R.; Lin, Z.; Zhang, M. Review on influencing factors of mechanical properties of fly ash geopolymer. *B. Chin. Ceram. Soc.* **2021**, *40*, 858–866. [CrossRef]
27. Jia, Y.; Zhang, Y.; Zhang, W. Preparation, properties and mechanism of slag based geopolymer. *J. Wuhan Univ. Techno.* **2009**, *31*, 120–125.
28. Lo, Y.; Lee, H. Curing effects on carbonation of concrete using a phenolphthalein indicator and Fourier-transform infrared spectroscopy. *Build. Environ.* **2002**, *37*, 507–514. [CrossRef]
29. Khan, H.A.; Castel, A.; Khan, M. Corrosion investigation of fly ash based geopolymer mortar in natural sewer environment and sulphuric acid solution. *Corros. Sci.* **2020**, *168*, 108586. [CrossRef]